

Electronic Supplementary Material (ESI) for JAAS.

This journal is © The Royal Society of Chemistry 2015

**Supplementary Information for**

**Probing Gas-phase Interactions of Peptides with “Naked” Metal**

**Ions**

Zhibin Yin, Rong Liu, Binwen Sun, and Wei Hang\*

Department of Chemistry and the MOE Key Lab of Spectrochemical Analysis & Instrumentation,  
College of Chemistry and Chemical Engineering, Xiamen University, Xiamen, China.

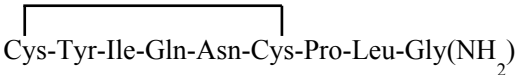
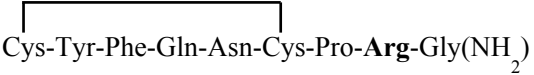
\*E-mail: [weihang@xmu.edu.cn](mailto:weihang@xmu.edu.cn)

## *Table of Contents*

1. Samples and Materials .....	3
2. Formation of Cu <sup>2+</sup> -Peptide Complexes in the Gas Phase .....	4
3. The Influence of Peptide/metal Ion Molar Ratio on the Yield of Metal-peptide Complexes .....	6
4. The Influence of Solution pH on the Yield of Metal-peptide Complexes .....	8
5. The Influence of Laser Energy on the Yield of Metal-peptide Complexes .....	9
6. Proof-of-Concept Calculation for Diffusion Model.....	10
7. Comparison of LI-ESI versus Conventional ESI for Gas-phase Stability of Metal-peptide Complexes.....	14
8. Mechanism for Collision-Induced Dissociation Processes .....	15

## 1. Samples and Materials

**Table S-1.** Information of the peptides used in the experiments

Peptide	Sequence
GHK	Gly-His-Lys
Non-Ac6	Ac-Leu-Ala-Ala-Ser-Leu-Gly (Ac-LAASLG)
Ac6	Ac-Leu- <b>Arg</b> -Ala-Ser-Leu-Gly (Ac-LRASLG)
Ac6 reversed sequence	Ac-leu-Ser-Ala- <b>Arg</b> -Leu-Gly (Ac-LSARLG)
Ac7	Ac-Leu- <b>Arg-Arg</b> -Ala-Ser-Leu-Gly (Ac-LRRASLG)
Ac7-2	Ac-Leu- <b>Arg-Arg-Arg</b> -Ser-Leu-Gly (Ac-LRRRSLG)
Oxytocin (OT)	 Cys-Tyr-Ile-Gln-Asn-Cys-Pro-Leu-Gly(NH <sub>2</sub> )
Vasopressin (VP)	 Cys-Tyr-Phe-Gln-Asn-Cys-Pro- <b>Arg</b> -Gly(NH <sub>2</sub> )
Angiotensin	Asp- <b>Arg</b> -Val-Tyr-Val- <b>His</b> -Pro-Phe
Bradykinin	<b>Arg</b> -Pro-Pro-Gly-Phe-Ser-Pro-Phe- <b>Arg</b>
Substance P (SP)	<b>Arg</b> -Pro- <b>Lys</b> -Pro-Gln-Gln-Phe-Phe-Gly-Leu-Met(NH <sub>2</sub> )
Substance P reversed sequence (Rev-SP)	Met-Leu-Gly-Phe-Phe-Gln-Gln-Pro- <b>Lys</b> -Pro- <b>Arg</b> (NH <sub>2</sub> )

## 2. Formation of $\text{Cu}^{2+}$ -Peptide Complexes in the Gas Phase

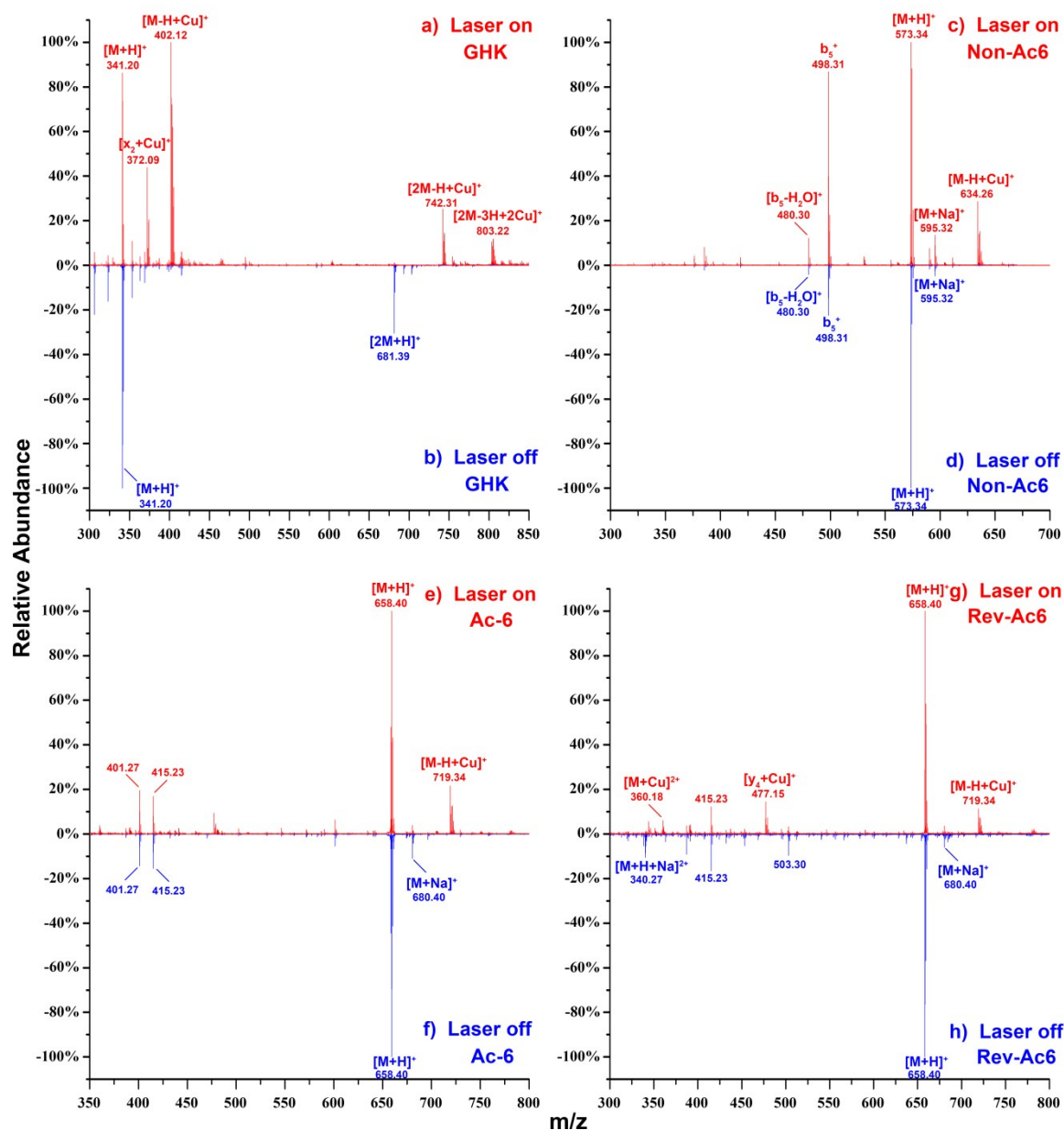


**Fig. S-1** Mass spectra of metal-peptide complexes generated in the gas phase involving various peptides and  $\text{Cu}^{2+}$ . The peptides are (a) Gly-His-Lys with and (b) without laser irradiance, (c) Ac-Leu-Ala-Ala-Ser-Leu-Gly with and (d) without laser irradiance, (e) Ac-Leu-Arg-Ala-Ser-Leu-Gly with and (f) without laser irradiance, and (g) Ac-Leu-Ser-Ala-Arg-Leu-Gly with and (h) without laser irradiance, respectively.

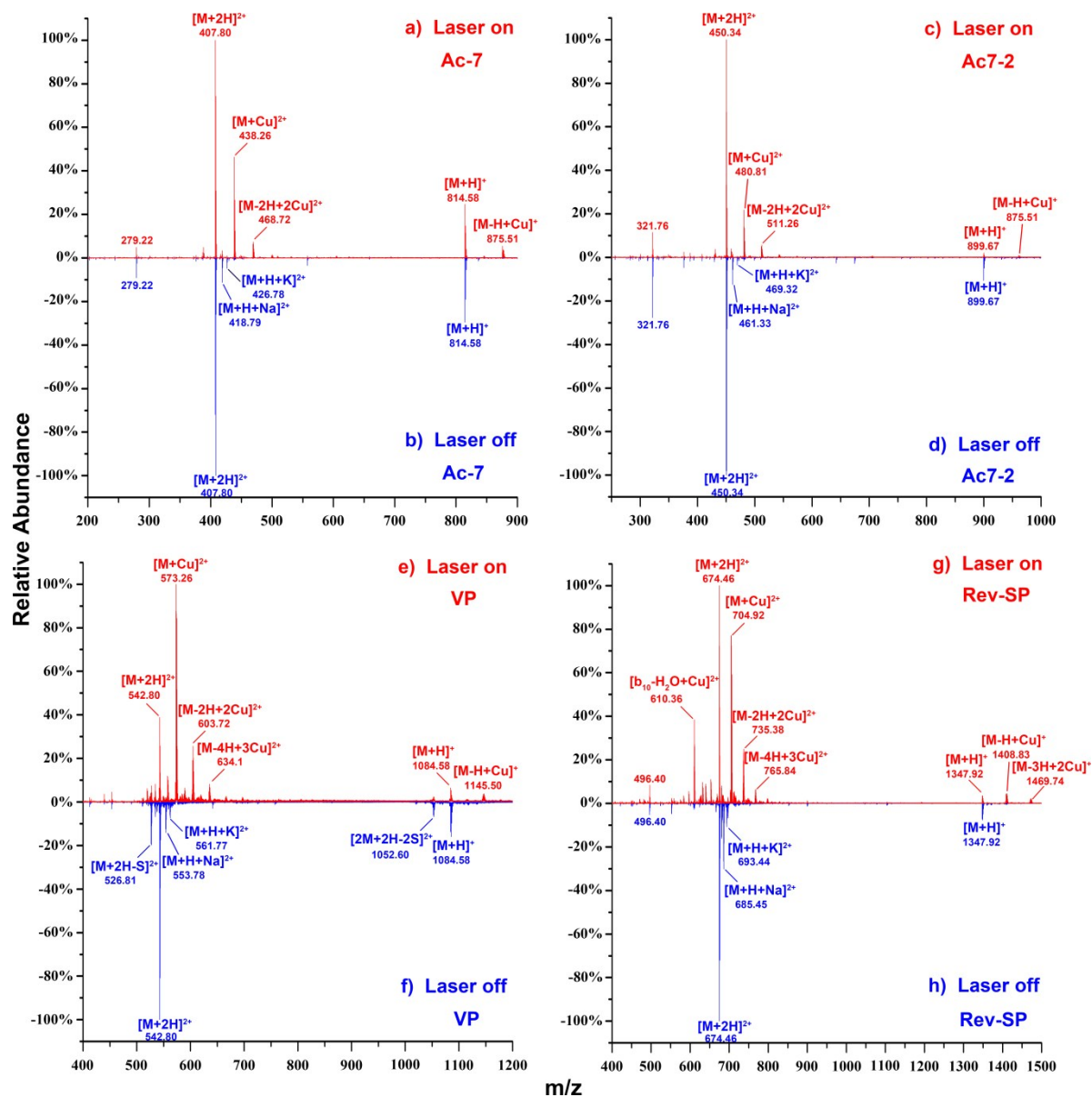


**Fig. S-2** Mass spectra of metal-peptide complexes generated in the gas phase involving various peptides and  $\text{Cu}^{2+}$ . The peptides are (a) Ac-Leu-Arg-Arg-Ala-Ser-Leu-Gly with and (b) without laser irradiance, (c) Ac-Leu-Arg-Arg-Arg-Ser-Leu-Gly with and (d) without laser irradiance, (e) VP with and (f) without laser irradiance, and (g) Rev-SP with and (h) without laser irradiance, respectively.

### 3. The Influence of Peptide/metal Ion Molar Ratio on the Yield of Metal-peptide Complexes

To investigate the influences of peptide/metal ion molar ratio on the yield of metal-ion peptide complexes, a 10  $\mu\text{M}$  peptide solution was added with 1  $\mu\text{M}$ , 10  $\mu\text{M}$ , 100  $\mu\text{M}$ , and 500  $\mu\text{M}$  metal salts solution to prepare peptide/metal ion complex solutions of 10:1, 1:1, 1:10, and 1:50, respectively. And  $\text{Cu}^{2+}$ -OT complexes with the molar ratio of 1:10, 1:1, 10:1, and 50:1 of peptide and  $\text{CuCl}_2$  solutions were produced directly by electrospray. As shown in Fig. S3b, the major ionic species are  $[\text{M}+\text{Cu}]^{2+}$  and  $[\text{M}-\text{H}+\text{Cu}]^+$  at 1:1 molar ratio of angiotensin and  $\text{Cu}^{2+}$ , while the binding of two or three  $\text{Cu}^{2+}$  ions to OT can be hardly observed. When the molar ratio is increased to 1:10 and 1:50, the signal of  $[\text{M}-2\text{H}+2\text{Cu}]^{2+}$  can be observed in addition to  $[\text{M}+\text{Cu}]^{2+}$  and  $[\text{M}-\text{H}+\text{Cu}]^+$ . However, the intensities of interference peak increase and signal-to-noise ratio of spectra drops, because signal suppression and dilution effects prevail to some extent (Fig. S3c-d). In compare with electrospray of Cu-peptide complexes with the molar ratio of 10:1, or even higher, of peptide and  $\text{CuCl}_2$  solutions, this method provides similar spectra avoiding signal suppression and dilution effects, which can be observed when high concentration of metal salts are added to peptide solution for electrospray (red boxes in Fig. S-3). Moreover, it can be anticipated that the ionization efficient of  $\text{Cu}^{2+}$  and reaction efficient of  $\text{Cu}^{2+}$  with peptides are quite high for the formation of  $[\text{M}+\text{Cu}]^{2+}$ ,  $[\text{M}-2\text{H}+2\text{Cu}]^{2+}$ , and  $[\text{M}-4\text{H}+3\text{Cu}]^{2+}$ .

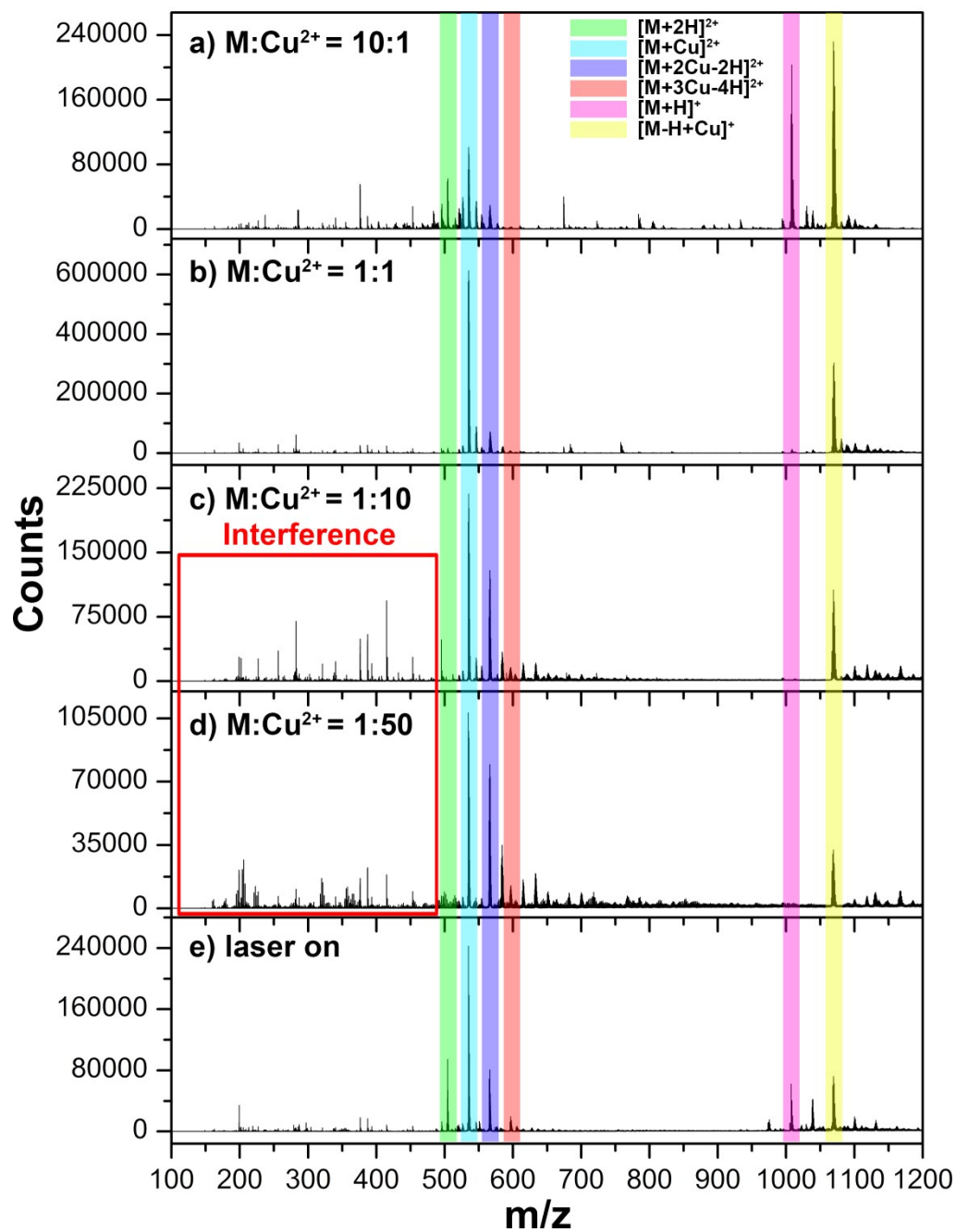


**Fig. S-3** The influence of OT/Cu<sup>2+</sup> molar ratio on the yield and species of metal-peptide complexes. Conventional ESI spectra at OT/Cu<sup>2+</sup> molar ratio of a) 10:1, b) 1:1, c) 1:10, d) 1:50 are compared with e) LI-ESI spectra distinctly.

## 4. The Influence of Solution pH on the Yield of Metal-peptide Complexes

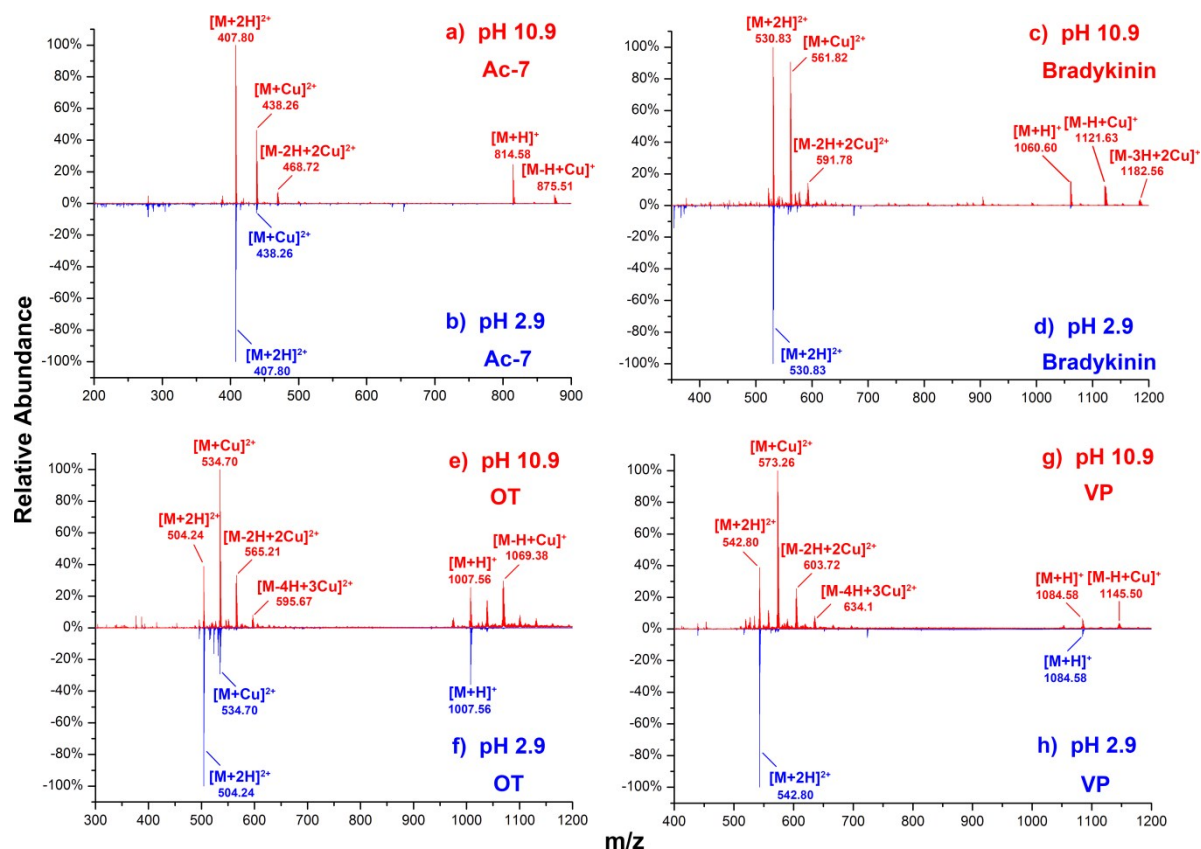


**Fig. S-4** LI-ESI spectra of Cu<sup>2+</sup>-peptide complexes with laser irradiance at different solution pH. The peptides are (a) Ac-Leu-Arg-Arg-Ala-Ser-Leu-Gly (Ac-7) buffered at pH 10.9 and (b) pH 2.9, (c) bradykinin buffered at pH 10.9 and (d) pH 2.9, (e) OT buffered at pH 10.9 and (f) pH 2.9, and (g) VP buffered at pH 10.9 and (h) pH 2.9, respectively.



## 5. The Influence of Laser Energy on the Yield of Metal-peptide Complexes

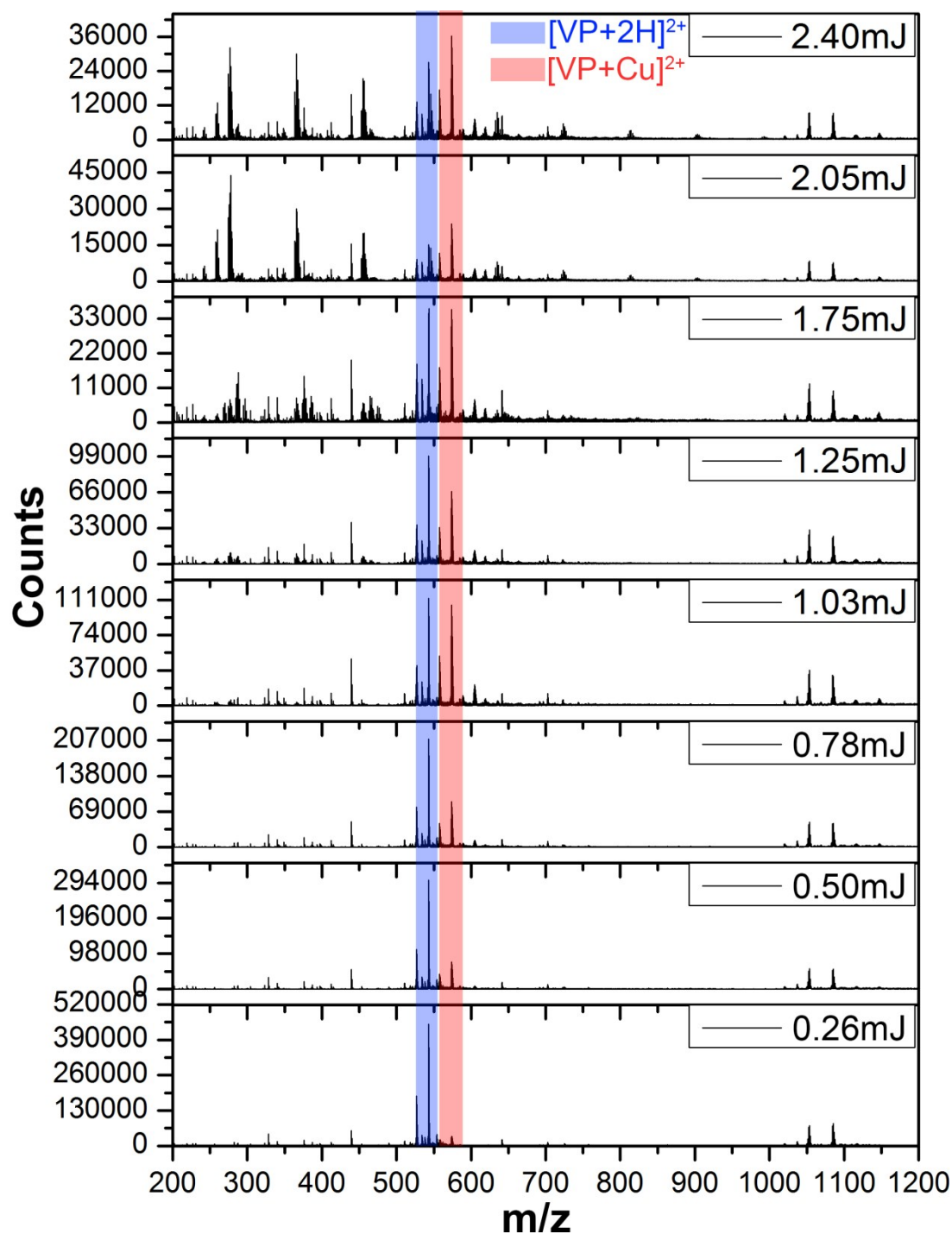


Fig. S-5 The influence of laser energy on the yield of  $Cu^{2+}$ -peptide complexes.

## 6. Proof-of-Concept Calculation for Diffusion Model

Laser ablation/ionization technique has been used extensively in solid sampling for elemental analysis, whereas the formation of metal ions with a few hundred nm-range mean free paths (MFPs) in open air for reaction or analysis directly is still a challenging issue. Although numerous models for laser-solid interaction operating in vacuum and at low pressure gas environment has been described,<sup>1, 2</sup> only a few models are presented in the literature for plume expansion in 1 atm background gas,<sup>3, 4</sup> even fewer models for expansion in open air. The interaction of laser with metal target, involving the plasma formation and plume expansion, is an intricate process. Compared to laser ionization in vacuum, interactions of plume with ambient gas is a far more complex gas-dynamic process. To better understanding the ionization mechanism of  $\text{Cu}^{2+}$ , it is necessary to calculate its MFP in open air. The MFP can be calculated by Equation S1,<sup>5</sup>

$$\lambda = \frac{kT}{\pi P(r_M + r_{N_2})^2} \quad (\text{S1})$$

where  $\lambda$  is the mean free path,  $k$  is Boltzmann constant,  $T$  is the thermal temperature (K),  $P$  is the pressure (Pa),  $r_M$  and  $r_{N_2}$  is the radius of an ablated metal atom and a nitrogen molecule (m), respectively. The MFP of Cu ion is calculated to about 137 nm in open air.

It is noteworthy that diffusion model has been extensively used for the study of glow discharge process, aiming at the sputtered sample atoms with little initial kinetic energy.<sup>6, 7</sup> Considering the calculated MFP of Cu ion is 137 nm in open air, all ions will experience thousands of collisions and lose their initial kinetic energy before arriving at 3 mm, mixing with background gas in the form of thermal motion according to the elastic collision model.<sup>8, 9</sup> Although the plume length by high irradiance LI is estimated to be 2.78 mm according to the studies by Gonzalo et al,<sup>10, 11</sup> it should be pointed out that the adiabatic free expansion is only in the early stage of plasma and accounts for a small part of the whole plume expansion. When concentrations of species are not uniform, diffusion process

will be dominant, promoting more Cu particles to pass in one direction towards electrospray emitter under the effect of concentration gradient. The transport of ablated atoms is believed to be governed by the diffusion process.<sup>6</sup>

For a three-dimensional spherical model, the density of particles at a distance  $r$  from the origin at time  $t$  can be calculated by the Equation S2.<sup>12</sup> Assuming at time  $t = 0$ , there are  $N$  particles ablated from the metal target. Under the high laser irradiance ( $\sim 10^{10} \text{ W cm}^{-2}$ ), the  $N$  can be estimated to  $4.2 \times 10^{15}$  based on the crater volume. The diffusion coefficient ( $D$ ,  $\text{cm}^2 \text{ s}^{-1}$ ) can be calculated by Equation S3

$$n(r,t) = \frac{N}{(4\pi Dt)^{3/2}} \exp\left(-r^2/4Dt\right) \quad (\text{S2})$$

$$D = \frac{3(2\pi k^3 T^3 / \mu)^{1/2}}{16P\pi\sigma^2} \quad (\text{S3})$$

Where  $k$  is Boltzmann constant,  $T$  is the thermal temperature (K),  $\mu$  is the reduced mass of the collision partners (kg),  $P$  is the pressure (Pa), and  $\sigma$  is the collision cross section ( $\text{cm}^2$ ). Under the experimental conditions, parameters of  $T = 298 \text{ K}$  and  $P = 101325 \text{ Pa}$  are used. Calculated Cu atom densities at several target-emitter distances as a function of time are shown in Fig. S-6. It can be seen that the atom density rises to a maximum after 20-30 ms, and decreases for a much longer period. Meanwhile, the shorter the distance, the higher the atom density can be obtained. However, discharge between electrospray emitter and metal target happen when the distance is less than 3.0 mm. Thus, the optimized distance of 3 mm was chosen. Considering the laser frequency is 10 Hz, the Cu atom density reaches value of  $4.6 \times 10^{15} \text{ cm}^{-3}$  at 3 mm and 0.1 s after the first laser pulse. At the moment, the second laser pulse irradiates metal target, the newly ablated Cu atoms can be follow-up and diffuse as aforementioned. The preceding Cu atoms at 3 mm can be ionized by the second laser pulse simultaneously. The focusing spot size at a height of 3 mm, where interaction of metal ions and molecules occurs, can be estimated to  $200 \mu\text{m}$ . The laser irradiance can reach  $7.2 \times 10^8 \text{ W cm}^{-2}$  at 3 mm, resulting in almost all the Cu atoms are ionized into  $\text{Cu}^+$  and  $\text{Cu}^{2+}$

with the fraction of about 50% and 50%.<sup>3, 13</sup> The densities of  $\text{Cu}^+$  and  $\text{Cu}^{2+}$  can reach values of  $2.3 \times 10^{15} \text{ cm}^{-3}$ .

To further verify the diffusion model is reasonable, the following equation was applied to calculate the peptide molecules density at the interaction area of metal ions and molecules:

$$N_t = (N_A \times c \times v \times t) / V \quad (\text{S2})$$

Where  $N_A$  is Avogadro constant,  $c$  is concentration of peptide solution,  $v$  is flow rate of syringe pump,  $t$  is time (0.1 s is used here),  $V$  is volume of the interaction area of metal ions and peptides. The calculated volume of cylinder (red marked area in Fig. S-7) is  $3.7 \times 10^{-6} \text{ cm}^3$ . Owing to the short distance between focused laser beam and emitter ( $\sim 0.5 \text{ mm}$ ), the cylinder can be approximated as the interaction area, where the calculated density of peptide molecules is  $5.4 \times 10^{15} \text{ cm}^{-3}$  in good agreement with that of  $\text{Cu}^{2+}$ . It can be inferred that all the interactive  $\text{Cu}^{2+}$  ions are ionized in the vicinity of the emitter. In fact, far higher densities of  $\text{Cu}^+$  and  $\text{Cu}^{2+}$  can be obtained, because continuously ablated Cu atoms can be accumulated with the increase of laser pulse numbers. For example, the accumulated Cu atom density at 3 mm reaches value of  $7.8 \times 10^{15} \text{ cm}^{-3}$  after 0.3 s, facilitating the high-efficiency interactions between  $\text{Cu}^{2+}$  ions with peptides. Hence, it is reasonable to account for the formation mechanism and high abundance of  $\text{Cu}^{2+}$  at interaction area as well as high yield of metal-peptide complexes by diffusion model.

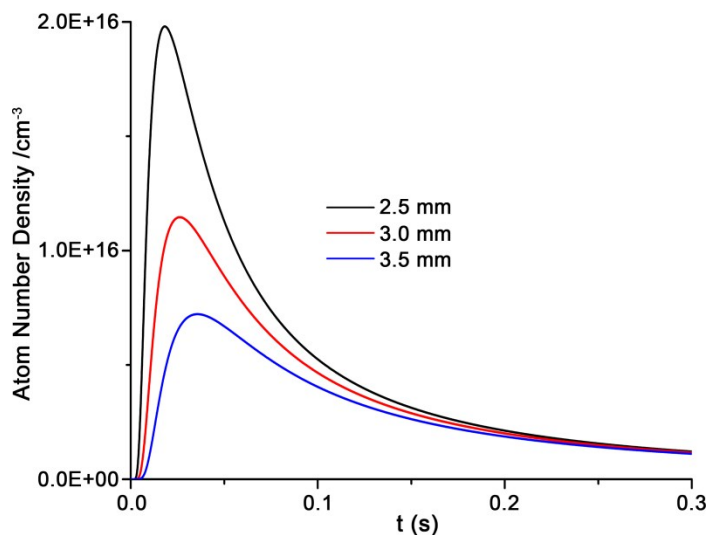


**Fig. S-6** Three-dimensional diffusion model of atom number density as a function of time at distances of 2.5 mm, 3.0 mm, and 3.5 mm, respectively.  $D$  is calculated to be  $0.572 \text{ cm}^2 \text{ s}^{-1}$  in open air.

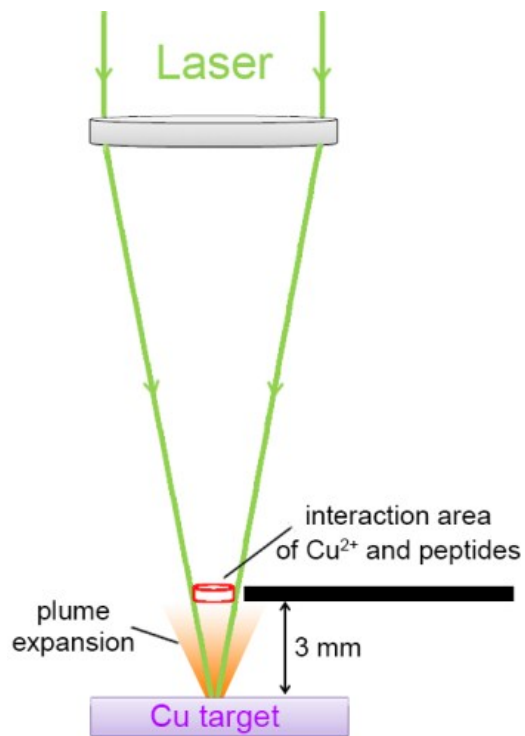


**Fig. S-7** Schematic diagram of the interaction area (red marked cylinder) of  $\text{Cu}^{2+}$  with peptides.

## 7. Comparison of LI-ESI versus Conventional ESI for Gas-phase

### Stability of Metal-peptide Complexes.

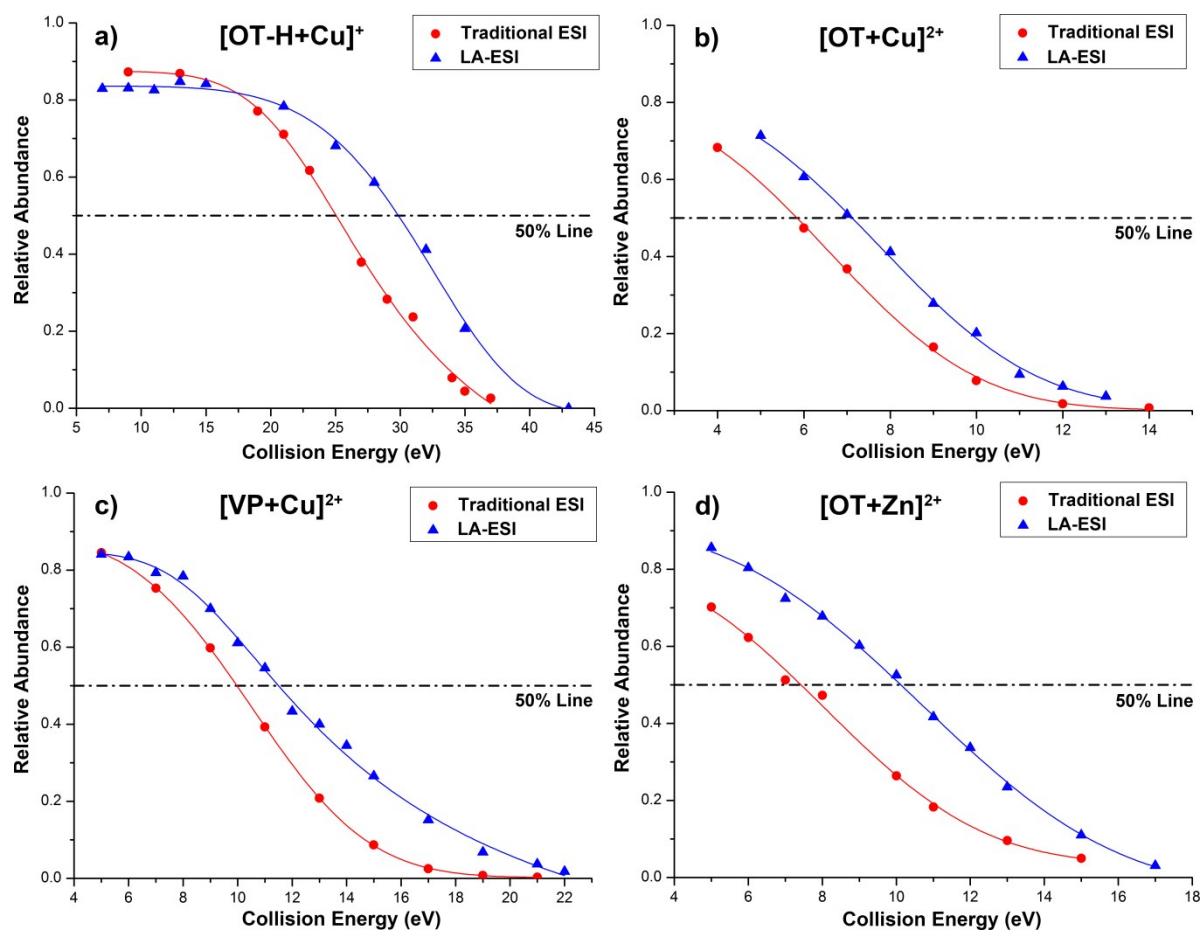
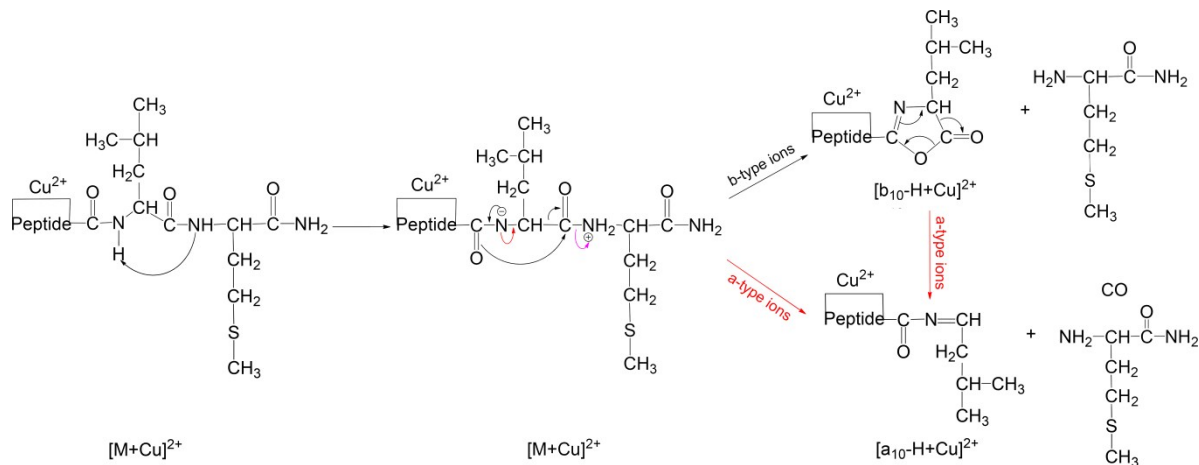
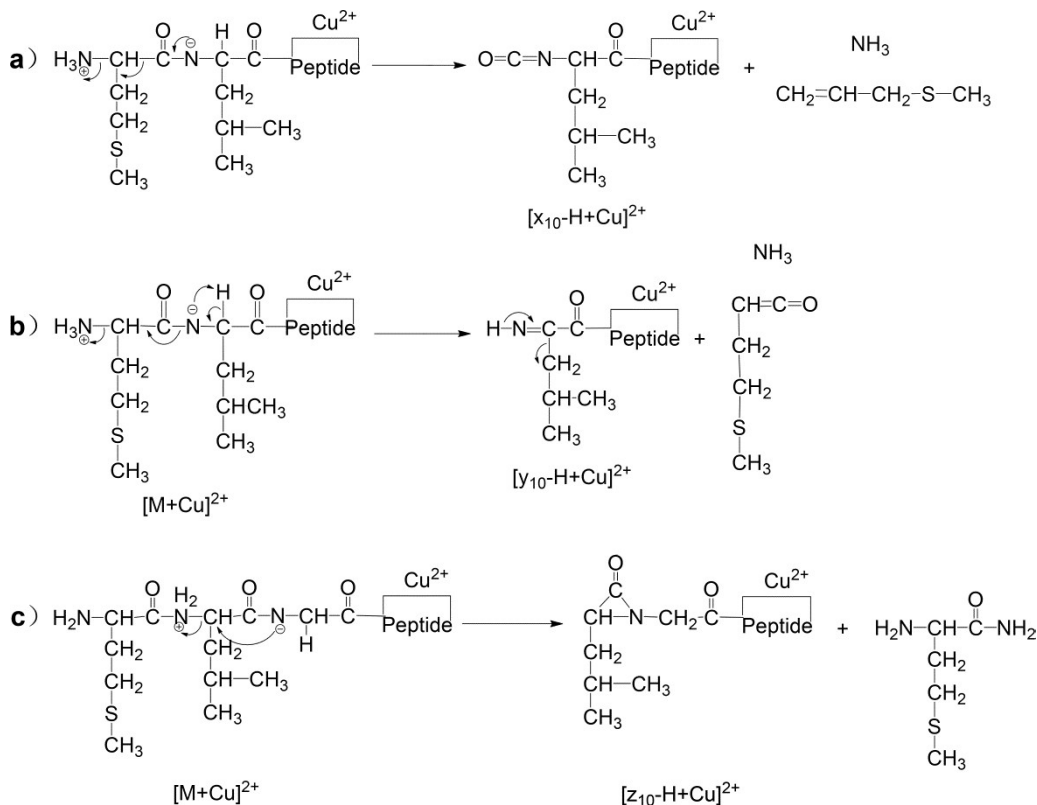


**Fig. S-8** Comparison of dissociation efficiency curves acquired by conventional ESI and LI-ESI for (a)  $[\text{OT-H+Cu}]^+$ , (b)  $[\text{OT+Cu}]^{2+}$ , (c)  $[\text{VP+Cu}]^+$ , (b)  $[\text{OT+Zn}]^{2+}$ . Relative abundance of  $[\text{M+Cu}]^{2+}$  are plotted as a function of collision energy. 50% lines (dot-dashed lines) corresponds to the collision energy associated with approximately 50% dissociation of  $[\text{M+Cu}]^{2+}$

## 8. Mechanism for Collision-Induced Dissociation Processes



**Scheme S-1.** Plausible CID mechanism for loss of residue 11 in  $[SP+Cu]^{2+}$  complexes yielding  $[a_6-H+Cu]^{2+}$  and  $[b_6-H+Cu]^{2+}$  (denoted as  $*a_6^{2+}$  and  $*b_6^{2+}$ , respectively).



**Scheme S-2** Plausible CID mechanism for loss of residue 1 in  $[M+Cu]^{2+}$  complexes yielding a)  $[x_{10}-H+Cu]^{2+}$  (denoted as  $*x_{10}^{2+}$ ), b)  $[y_{10}-H+Cu]^{2+}$  (denoted as  $*y_{10}^{2+}$ ), and c)  $[z_{10}-H+Cu]^{2+}$  (denoted as  $*x_{10}^{2+}$ ,

\* $\text{Y}_{10}^{2+}$ , and \* $\text{Z}_{10}^{2+}$ , respectively), for M = Rev-SP.

## References

1. A. Bogaerts, Z. Chen, R. Gijbels and A. Vertes, *Spectrochim. Acta Part B*, 2003, **58**, 1867-1893.
2. S. S. Harilal, C. V. Bindhu, M. S. Tillack, F. Najmabadi and A. C. Gaeris, *J. Appl. Phys.*, 2003, **93**, 2380-2388.
3. Z. Chen and A. Bogaerts, *J. Appl. Phys.*, 2005, **97**, 063305.
4. A. Bogaerts, Z. Chen and D. Bleiner, *J. Anal. At. Spectrom.*, 2006, **21**, 384-395.
5. X. Y. Chen, S. B. Xiong, Z. S. Sha and Z. G. Liu, *Appl. Surf. Sci.*, 1997, **115**, 279-284.
6. M. Van Straaten, R. Gijbels and A. Vertes, *Anal. Chem.*, 1992, **64**, 1855-1863.
7. W. Hang and W. W. Harrison, *Anal. Chem.*, 1997, **69**, 4957-4963.
8. S. Amoruso, B. Toftmann and J. Schou, *Appl. Phys. A*, 2004, **79**, 1311-1314.
9. S. Amoruso, B. Toftmann and J. Schou, *Phys. Rev. E*, 2004, **69**, 056403.
10. J. Gonzalo, R. Gómez San Román, J. Perrière, C. N. Afonso and R. Pérez Casero, *Appl. Phys. A*, 1998, **66**, 487-491.
11. P. E. Dyer, A. Issa and P. H. Key, *Appl. Phys. Lett.*, 1990, **57**, 186-188.
12. A. M. Howatson, *An Introduction to Gas Discharges*, Pergamon Press, 1976.
13. A. Bogaerts and Z. Chen, *Spectrochim. Acta Part B*, 2005, **60**, 1280-1307.